Available online at www.sciencedirect.com
ScienceDirect
Journal of Energy Chemistry 23(2014)483–490
JOURNAL OF ENERGY CHEMISTRY
www.elsevier.com/journals/journal-of-energy-chemistry/2095-4956
www.elsevier.com/locate/jngc

Synthesis of Pt and Pt-Fe nanoparticles supported on MWCNTs used as electrocatalysts in the methanol oxidation reaction

J. R. Rodriguez[a*], R. M. Félix[b], E. A. Reynoso[b], Y. Gochi-Ponce[c], Y. Verde Gómez[d], S. Fuentes Moyado[a], G. Alonso-Núñez[a]

a. Universidad Nacional Autónoma de México, Centro de Nanociencias y Nanotecnología, Ensenada, B. C., C. P. 22860, Mexico;
b. Instituto Tecnológico de Tijuana, Centro de Graduados e Investigación, Tijuana, B. C., C. P. 22000, Mexico;
c. Instituto Tecnológico de Oaxaca, Departamento de Ingeniería Química y Bioquímica, Oaxaca, Oax., C. P. 68030, Mexico;
d. Instituto Tecnológico de Cancún, Av. Kabah Km. 3, Cancún, Q. R., C. P. 77500, Mexico

[Manuscript received October 24, 2013; revised January 13, 2014]

Abstract

This work reports a feasible synthesis of highly-dispersed Pt and Pt-Fe nanoparticles supported on multiwall carbon nanotubes (MWCNTs) without Fe and multiwall carbon nanotubes with iron (MWCNTs-Fe) which applied as electrocatalysts for methanol electrooxidation. A Pt coordination complex salt was synthesized in an aqueous solution and it was used as precursor to prepare Pt/MWCNTs, Pt/MWCNTs-Fe, and Pt-Fe/MWCNTs using $FeCl_2{\cdot}4H_2O$ as iron source which were named S1, S2 and S3, respectively. The coordination complex of platinum $(TOA)_2PtCl_6$ was obtained by the chemical reaction between $(NH_4)_2PtCl_6$ with tetraoctylammonium bromide (TOAB) and it was characterized by FT-IR and TGA. The materials were characterized by Raman spectroscopy, SEM, EDS, XRD, TEM and TGA. The electrocatalytic activity of Pt-based supported on MWCNTs in the methanol oxidation was investigated by cyclic voltammetry (CV) and chronoamperometry (CA). Pt-Fe/MWCNTs electrocatalysts showed the highest electrocatalytic activity and stability among the tested electrocatalysts due to that the addition of "Fe" promotes the OH species adsorption on the electrocatalyst surface at low potentials, thus, enhancing the activity toward the methanol oxidation reaction (MOR).

Key words

coordination complex salt; MWCNTs; nanoparticles; catalysts; electrooxidation

1. Introduction

Nowadays the direct methanol fuel cells (DMFCs) have attracted considerable attention as a power source for zero emission electric vehicles and portable electronic devices due to their high efficiencies and environmental friendliness [1,2]. Unfortunately, the sluggish anodic methanol oxidation reaction (MOR) catalyzed in the anode by Pt electrocatalysts and the high cost of the noble metal, are some problems which should be overcome [3]. Therefore it is imperative for the development of new electrocatalytic materials with high efficiencies and low costs [4]. Currently, the strategies adopted to improve the catalysts performance and cost-efficiency include the synthesis of new low loading Pt-based electrocatalysts [5], the development of better catalyst supports [6], and the searching of new alternatives of Pt-free active metals [7,8]. Although the use of the non-Pt electrocatalysts is attractive, its application for the oxidation of small organic molecules in fuel cell is still far yet to occur [9]. In recent years the electrocatalysts of Pt nanoparticles coupled with transition metals such as Ru, Au, and Fe have been tested to improve the electrocatalytic activity in MOR [10−12]. Besides, in the last years, the multiwall carbon nanotubes (MWCNTs) have been applied as an alternative support for metal catalysts [13]. It has been found that MWCNTs can provide better electrochemical performances as catalyst supports on the fuel cells in comparison with traditional carbon supports (carbon black) [14,15]. Its excellent stability in acid media and its high electrical conductivity can be the main factors responsible for such findings [16]. On the other hand, Alonso-Nuñez et al. [17] and J. R. Rodriguez et al. [18] reported the synthesis of coordination complexes salts with different noble metals used as precursors of nanostructures supported on MWCNTs. In this direction, the present work also describes the synthesis of a Pt coordination

* Corresponding author. Tel: +52-646-1744602; E-mail: jrodrig@cnyn.unam.mx
This work was supported by CONACyT (Project 155388 and 174689).

doi: 10.1016/S2095-4956(14)60175-3

complex salt, $(TOA)_2PtCl_6$, which was characterized by FT-IR and TGA. The salt was used to prepare nanoparticles (NPs) of Pt and Pt-Fe supported on MWCNTs to be used as electrocatalysts for MOR. In this report we also studied the effects of the incorporation of iron in the Pt/MWCNTs for the MOR. The materials were characterized by SEM, EDS, TEM, XRD and TGA. Finally, the electrocatalysts were studied by cyclic voltammetry (CV) and chronoamperometry (CA) in the MOR.

2. Experimental

The chemicals reagents used in this study, $(NH_4)_2PtCl_6$, $FeCl_2{\cdot}4H_2O$ and $(C_5H_5)_2Fe$ were acquired from Alfa Aesar and $NaBH_4$, TOAB (tetraoctylammonium bromide), toluene and 2-propanol were purchased from Aldrich Co. All chemicals were used without further purification.

2.1. Synthesis of Pt precursor: $(TOA)_2PtCl_6$

The coordination complex salt of Pt was synthesized using the Burst-Schiffrin method [19]. First, the ammonium hexachloroplatinate (IV), $(NH_4)_2PtCl_6$, (0.2 g, 4.5×10^{-4} mol) was dissolved into 10 mL triply distilled water. This aqueous solution was then added to 15 mL of a TOAB (0.493 g, 9.0×10^{-4} mol) in 2-propanol solution at room temperature at 25 °C. The resulting solution was left under stirring until the complete precipitation of $(TOA)_2PtCl_6$ according to Equation (1). The product was filtered under vacuum, washed with deionized water, and dried at 70 °C for 8 h. The yield of $(TOA)_2PtCl_6$ was 86%.

$$(NH_4)_2PtCl_6+2TOAB\longrightarrow(TOA)_2PtCl_6+2(NH_4)Br \quad (1)$$

2.2. Synthesis of MWCNTs

The MWCNTs were synthesized by the spray pyrolysis method, reported elsewhere [20]. First, a starting solution composed of 1.0 g ferrocene into 25 mL toluene was prepared. This was atomized and carried by an argon flow into a Vycor tube which was heated in a cylindrical furnace equipped with a high precision temperature controller (±1 °C). The furnace temperature was set at 900 °C and the flow rate was regulated to 75 mL/s. The solution was fed for 30 min. Then a black film of MWCNTs-Fe was formed on the inner surface of the Vycor tube and it was mechanically removed and collected. The raw MWCNTs-Fe (0.5 g) was used to support Pt nanoparticles obtaining the sample named S1. On the other hand, to prepare S2 and S3 electrocatalysts, MWCNTs were treated in order to decrease the Fe content, as follows: 0.5 g MWCNTs-Fe as prepared was added to 20 mL HNO_3 solution (Aldrich, 70%). The mixture was placed in an ultrasonic bath for 1 h and then stirred for 12 h while refluxed. The product was filtered under vacuum, washed with deionized water, and dried at 70 °C for 8 h; since then they will be called MWCNTs.

2.3. NPs/MWCNTs

The in situ synthesis of nanoparticles (NPs) on the MWCNTs surface from metallic precursors $(TOA)_2PtCl_6$ and $FeCl_2{\cdot}4H_2O$, is described in the following sections.

2.3.1. Pt/MWCNTs-Fe (S1)

Raw MWCNTs-Fe (25 mg) were added to 2-propanol (25 mL) and dispersed in an ultrasonic bath for 1 h. In a second step, 3.13×10^{-5} mol Pt precursor ($(TOA)_2PtCl_6$) dissolved in 5 mL 2-propanol solution were added to the MWCNTs-Fe suspension and stirred for 1 h. Finally, 10 mL aqueous solution of $NaBH_4$ in excess (stoichiometric metal ratio : $NaBH_4$, 1 : 10) was added by drip during 5 min to the suspension, which was stirred at room temperature for 12 h to reduce Pt^{4+} to Pt^0. The obtained mixture was then filtered and washed with acetone and water, to be finally dried at 70 °C for 4 h. The chemical reduction reaction that occurs during the Pt/MWCNTs-Fe synthesis is shown in Equation 2.

$$(TOA)_2PtCl_6+\text{MWCNT-Fe}+BH_4^-\longrightarrow\text{Pt/MWCNT-Fe} \quad (2)$$
$$(\text{Solution: } (TOA)^+Cl,\ NaCl,\ B(OH)_3)$$

2.3.2. Pt/MWCNTs (S2)

MWCNTs treated (25 mg) were added to 2-propanol (25 mL) and dispersed in an ultrasonic bath for 1 h. As a second step a solution of 3.13×10^{-5} mol $(TOA)_2PtCl_6$ in 5 mL 2-propanol was prepared. Then this solution was mixed to the MWCNTs suspension and stirred for 1 h. Finally, 10 mL aqueous solution of $NaBH_4$ in excess (stoichiometric metal ratio : $NaBH_4$, 1 : 10) was added by drip during 5 min to the suspension, which was stirred at room temperature for 12 h. The obtained mixture was then filtered and washed with acetone and water and finally dried at 70 °C for 4 h. The propose reaction to obtain Pt/MWCNTs is shown in Equation (3).

$$(TOA)_2PtCl_6+\text{MWCNTs}+BH_4^-\longrightarrow\text{Pt/MWCNTs} \quad (3)$$
$$(\text{Solution: } (TOA)^+Cl,\ NaCl,\ B(OH)_3)$$

2.3.3. Pt-Fe/MWCNTs (S3)

MWCNTs cleaned (25 mg) were added to 25 mL 2-propanol and dispersed in an ultrasonic bath for 1 h. In a second step, 3.13×10^{-5} mol metals (Pt : Fe ratio of 1 : 1) from $(TOA)_2PtCl_6$ and $FeCl_2$ as precursors were dissolved in 5 mL 2-propanol. Then this solution was added to the MWCNTs suspension and stirred for 1 h. Finally in the third step, 10 mL aqueous solution of $NaBH_4$ in excess (stoichiometric metal : $NaBH_4$ ratio of 1 : 10) was added by drip during 5 min to the suspension, which was stirred at room temperature for 12 h. The obtained mixture was then filtered, to be later washed with acetone and water, and finally dried at 70 °C

for 4 h. In this step, the chemical reduction reaction occurs to obtain Pt-Fe/MWCNTs as shown in Equation (4).

$$(TOA)_2PtCl_6+Fe^{2+}+MWCNTs+BH_4^- \longrightarrow \text{Pt-Fe/MWCNTs} \quad (4)$$
$$(\text{Solution: } (TOA)^+Cl, NaCl, B(OH)_3)$$

2.4. Electrode preparation

The electrocatalytic inks were prepared by thoroughly mixing 2 mg of each sample Pt/MWCNTs-Fe (S1) Pt/MWCNTs (S2) or Pt-Fe/MWCNTs (S3) with 150 μL of Nafion ionomer (Aldrich, 5%) and 550 μL of ethanol (Aldrich, 99.5%). The mixture was placed in an ice bath to prevent overheating and to minimize the evaporation of the solvent, and then ultrasonically mixed for 180 s. A 5 μL aliquot of these inks was deposited using a micro-pipette onto a freshly polished glassy carbon (GC) electrode (3 mm in diameter). After the solvent was evaporated at 40 °C, the electrode was used as a working electrode. S1, S2 and S3 working electrodes contained about 4.97×10^{-4}, 4.97×10^{-4}, and 2.49×10^{-4} mmol Pt, respectively.

2.5. Characterization

The coordination complex salt was characterized by infrared spectroscopy (FT-IR) using a Perkin-Elmer FT-IR 1605 spectrometer. It was also characterized by thermogravimetric analysis (TGA) using a TA-Instruments SDT 2920. The sample was heated in a platinum-pan under dry air flux from room temperature up to 700 °C with a heating rate of 5 °C/min.

The MWCNTs were characterized by Raman spectroscopy using a J. Y. Horiba LabRam-HR system interfaced with an Olympus BX41 optical microscopy and an Ar laser (Olympus TH4-100, 20 mW at 532 nm) source.

The morphology of the NPs/MWCNTs was studied by scanning electron microscopy (SEM) using a JEOL JSM5300 with accelerating voltage of 15 kV. The sample composition content was determined by means of a JEOL JSM5300 equipped with a Kevex Super Dry EDS (energy disperse spectroscopy), with scan range of 0 to 10 keV. NPs/MWCNTs were studied by X-ray diffraction (XRD) using a Phillips X'Pert Diffractometer, with Cu K_α (λ=1.5405 Å) radiation source operated at 45 kV and 40 mA. All samples were evaluated in a 2θ range from 10° to 80°; crystalline phases were identified using the database JCPDS-ICDD 2003 files. The morphology and size of the NPs were investigated by transmission electron microscopy (TEM) using a JEOL 2010 microscope. Also TGA studies were performed for the electrocatalyst in an air atmosphere where the samples were heated at 5 °C/min from room temperature to 700 °C. Electrochemical measurements were performed using an EC Epsilon BAS potentiostat/galvanostat in a conventional three electrode electrochemical cell, using a GC electrode as a working electrode, Pt electrode as a counter electrode and an Ag/AgCl electrode as a reference electrode. Electrochemical experiments included CV and CA measurements which were carried out at room temperature. Before each experiment, the GC electrode was mechanically polished with alumina (0.05 μm, Buehler) and rinsed with ultrapure water to remove the impurities. Before the MOR took place, the surface of the working electrode was cleaned with a 0.5 mol/L H_2SO_4 solution saturated with N_2 for 10 cycles between −0.2 V and 1.3 V at 100 mV/s [21,22]. For the MOR a 0.5 mol/L H_2SO_4+1.0 mol/L MeOH solution saturated with N_2 was used and the cyclic voltammograms were performed at 100 mV/s between −0.2 V and 1.3 V for 10 cycles [23,24]. The electrolyte solutions of 0.5 mol/L H_2SO_4 and 1 mol/L MeOH were prepared using H_2SO_4 (Fermont, 98%), methanol (Aldrich, 99.5%) and ultrapure water (Millipore MilliQ, 18 M ·cm).

3. Results and discussion

3.1. Characterization of the organometallic salts

3.1.1. FT-IR study

Figure 1 shows the infrared spectrum corresponding to the $(TOA)_2PtCl_6$ structure, whereas Table 1 summarizes the infrared frequencies detected for the organometallic precursor with its corresponding vibration modes. The IR spectrum of $(TOA)_2PtCl_6$ presents four main groups of vibration attributed to the TOA group at 725, 1481, 2853, and 2924 cm^{-1}. The band observed at 725 cm^{-1} corresponds to a rocking mode vibration of the CH_2 chain. The band observed at 1481 cm^{-1} is defined as the asymmetric C–H scissoring vibration of the CH_2–N^+, whereas the bands at 2924 and 2853 cm^{-1} are assigned to the asymmetric and symmetric C-H respectively, due to stretching vibrations of the methylene (CH_2) group of the TOA. These bands are similar to those obtained by the pure TOAB molecule [25].

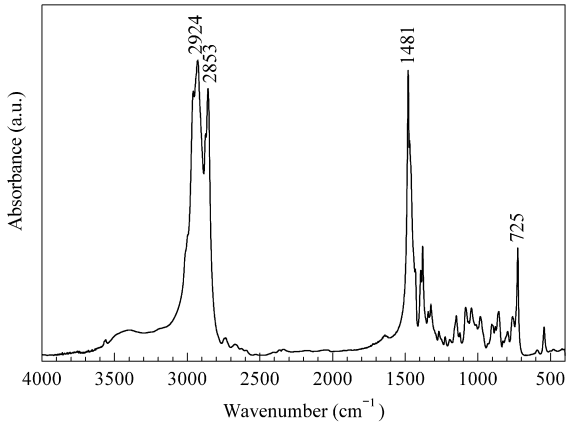

Figure 1. IR spectrum of the $(TOA)_2PtCl_6$ compound

Table 1. FT-IR frequencies observed for the $(TOA)_2PtCl_6$ compound

Compounds	IR frequencies (cm^{-1})			
	υ_{as} (CH_2)	υ_s (CH_2)	δ(C–H) of N–$(CH_2)_4$	β-(CH_2)
$(TOA)_2PtCl_6$	2924	2853	1481	725
TOAB [25]	2925	2859	1458	714

3.1.2. TGA study

Figure 2 shows the thermal decomposition behavior of the $(TOA)_2PtCl_6$ salt, while Table 2 summarizes the weight loss detected in each decomposition step of the organometallic precursor. Two steps of weight loss can be distinguished at average temperatures of 240−350 °C and 350−480 °C. The first step corresponds to the loss of the main parts of the hydrocarbons $8(CH_3(CH_2)_5CH{=}CH_2)$ with a weight loss of 66% (theoretical 66%). The second step corresponds to the loss of $2NH_4Cl$ in combination with two chlorine molecules ($2Cl_2$) leading to a weight loss of 16% (theoretical 18%). The chemical formula of the residue gives PtO_2 with 18% (theoretical 17%) suggesting that Pt is remaining in an oxidation state of IV. The discrepancies between the theoretical and experimental weight losses were −1.0%, due to the possible presence of $(NH_4)_2PtCl_6$ that did not react with TOAB.

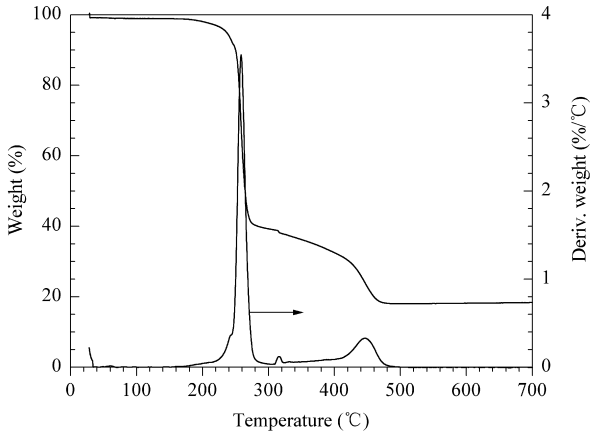

Figure 2. Weight loss and the first derivative curves recorded from TGA analysis of $(TOA)_2PtCl_6$ compound under oxygen

Table 2. TGA results of $(TOA)_2PtCl_6$ compound under oxygen atmosphere

	$(TOA)_2PtCl_6$
T_1 (°C)	240−350
w_1 (wt%, exp.)	66
w_1 (wt%, theor.)	66
Assuming loss	$8(CH_3(CH_2)_5CH{=}CH_2)$
T_2 (°C)	350−480
w_2 (wt%, exp.)	16.0
w_2 (wt%, theor.)	18.0
Assuming loss	$2Cl_2{+}2NH_4Cl$
w, (wt%, exp.)	82.0
Residual (wt%, exp.)	18.0
Residual (wt%, theor.)	17.0

Assuming residual as PtO_2

3.2. Raman spectroscopy study of MWCNTs

Raman spectrum provides further information about the crystallinity and morphology of the MWCNTs. Two strong peaks at 1587 and 2703 cm^{-1} and one weak peak at 1361 cm^{-1} are observed in the Raman spectra of Figure 3. The peak at 1587 cm^{-1} is attributed to the vibration of sp^2-bonded carbon atoms which is commonly named first-order G-band, and corresponds to the tangential vibrations of the carbon atoms [26,27]. The small peak at 1361 cm^{-1} is assigned to the vibration of the D-band carbon atoms with dangling bonds in plane terminations of the disorder [26−28]. The peak at 2703 cm^{-1} is an overtone or second-order harmonic of the G mode assigned to G'-band and the intensity of this peak depends strongly on the metallicity of the nanotube [29−31]. The lower value of I_D/I_G corresponds to better quality tubes. The I_D/I_G ratio for raw MWCNTs-Fe and MWCNTs comes out to be 0.28 and 0.34, respectively. The higher value of I_D/I_G may be due to the presence of amorphous carbon and defects of the sample [27].

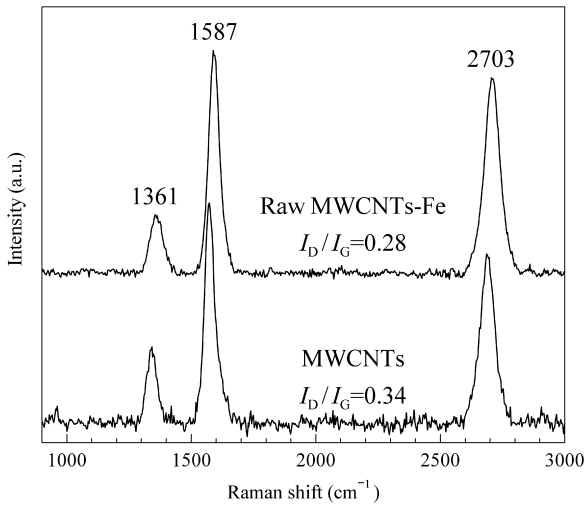

Figure 3. Raman spectra of MWCNTs and MWCNTs-Fe after treatment with HNO_3

3.3. Nanoparticles on MWCNTs

3.3.1. SEM and EDS study

The chemical composition of the NPs/MWCNTs was examined by EDS analysis, and the spectrum is given in Figure 4(c). The elemental quantification was done using the standard Magic 5 software, and results in atomic percent are shown in Table 3. The morphologic information of the electrocatalysts was studied by SEM analysis. Figure 4 represents the typical SEM micrograph of the samples, In Figure 4(a) and 4(b), rodlike morphology can be seen with a diameter in the nanometer range and length varying in some micrometer.

Figure 4. SEM images of raw MWCNTs-Fe (a); Pt-Fe/MWCNTs (b) and its EDS spectrum (c)

Table 3. Bulk chemical composition of the analyzed samples

Samples	Content (at%)	
	Pt	Fe
S1	43.3	56.7
S2	98.8	1.2
S3	55.8	44.2

3.3.2. XRD study

Crystallographic information of the electrocatalysts was obtained by powder X-ray diffraction technique. The XRD patterns (Figure 5) for S1, S2 and S3 catalysts show three diffraction peaks at the Bragg angles of 39.8°, 46.2° and 67.5° that correspond to the (111), (200) and (220) planes of Pt, reported on the database JCPDS file No. 04−0802. The diffraction peak at 26.4° corresponds to the (002) plane of C support, reported on the database JCPDS file No. 08−0415. The diffraction peak at 54.5° corresponds to the (112) plane of PtO, reported on the database JCPDS file No. 85−0714 [32]. No Fe^0 or Fe_2O_3 peaks are observed in the XRD patterns of all samples and this is probably because their phases were not fully developed. It may also be that the particle sizes of Fe were relative small or probably the Fe atoms were incorporated in the Pt structure forming an alloy. Table 4 lists the calculated average sizes for all the catalysts nanoparticles supported on MWCNTs, which were calculated from the Pt (111) peak using the Scherer equation [33,34].

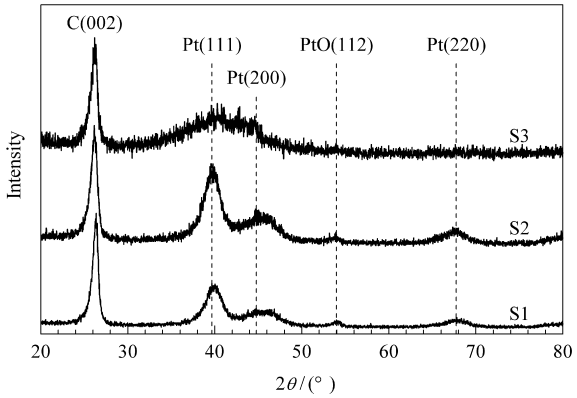

Figure 5. XRD patterns of three electrocatalysts

$$d = 0.9\lambda/(B\cos\theta) \qquad (5)$$

where, d is the average particle sizes (nm), λ is the wavelength of X-ray radiation (Cu K_α, $\lambda_{K_{\alpha 1}}$ = 1.5418 Å), θ is the angle at the position of the peak maximum and B is the half peak broadening for Pt (111) peak.

3.3.3. TEM study

Figure 6 shows TEM micrographs of the Pt and Pt-Fe

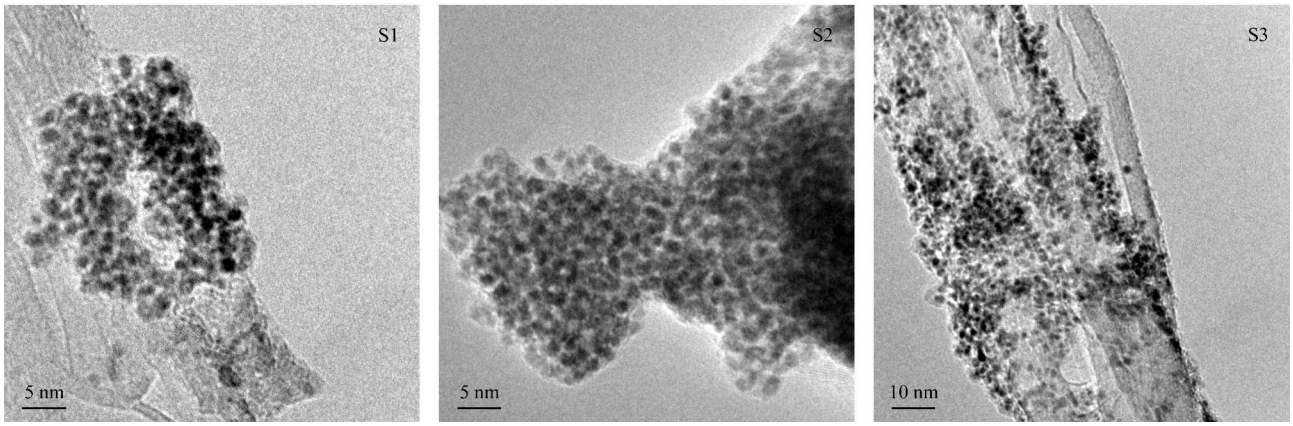

Figure 6. TEM images of three electrocatalysts at low magnifications

nanoparticles supported on MWCNTs. It can be seen that for all samples the NPs were formed uniformly on the external wall of the CNTs, showing spherical morphologies for all samples. The micrographs showed well-dispersed metal nanoparticles on the MWCNTs. Their sizes were obtained by measuring the nanoparticles from TEM images using a digital micrograph imaging analysis software (Gatan, Inc). More than 100 nanoparticles were measured to ensure the statistically significant representation of the nanoparticles sizes. All samples had a mean size of less than 4 nm. The size distributions of these NPs according with the TEM images (Figure 6) are fairly consistent with the Gaussian distribution, obtaining an average size of 2.1±0.5, 1.7±0.4 and 1.5±0.2 nm for the samples S1, S2, and S3, respectively. Thus, these values of the particle size (Table 4) are slightly different to those obtained by XRD analysis, but they follow the same pattern.

Table 4. Average particle sizes of three electrocatalysts based on XRD and TEM

Samples	XRD particle size (nm)	TEM particle size (nm)
S1	3.4	2.1±0.5
S2	3.2	1.7±0.4
S3	1.5	1.5±0.2

3.3.4. TGA study

TGA were performed under dry air flux for all samples to quantify the amount of metal deposited on the support. Figure 7 shows the different TGA curves obtained for each one of the samples, whereas quantification results as well as onset and final temperatures for the oxidation (T_{oxid}) process are listed in Table 5. For S1 (solid line), support oxidation starts at 463 °C and finalizes at 665 °C. Only a residual mass of 25.6 wt% was founded corresponding to PtO_2 and Fe_2O_3 coming from Pt NPs and remaining ferrocene, respectively. The residual mass for the sample S2 was of 14.7 wt%, which corresponds to PtO_2 coming from the coordination complex salt of Pt. The residual mass for the sample S3 was of 22.3 wt% and it corresponds to PtO_2 and Fe_2O_3 coming from the precursor salts. The sample S3 was the most effective toward the oxidation of the MWCNTs as a result of the oxygen species formed on Pt-Fe which are transferred to the carbon surface as a result of the intimate contact between Pt-Fe nanoparticles and the carbon, which is derived from the formation of CO_2. Pt-Fe is definitely oxidized into PtO_2 and Fe_2O_3 only after the complete oxidation of the carbon support [35]. It is also shown in Table 5 that the raw MWCNTs-Fe and MWCNTs oxidation starts at 460 °C and finalizes at 670 and 680 °C, respectively. Only a residual mass of 10.5 wt% by the raw MWCNTs-Fe and 0.5 wt% by the MWCNTs were founded corresponding to Fe_2O_3 coming from remaining ferrocene, respectively.

Table 5. TGA results for the Pt-M/MWCNTs systems decomposition under oxygen atmosphere

Samples	Onset T_{oxid} (°C)	Final T_{oxid} (°C)	Residual metal oxide amount (wt%)
S1	463	665	25.6
S2	426	655	14.7
S3	400	630	22.3
MWCNTs-Fe	460	670	10.5
MWCNTs	460	680	0.5

3.4. Electrochemical evaluation

Figure 8 shows that CV curves are similar to those of pure polycrystalline Pt. However, the hydrogen adsorption/desorption region presented a shift to higher potentials for S3. This is due to an interaction from Pt-Fe, causing changes in the adsorption strength of the hydrogen on the Pt, because the Pt-Fe material is more electropositive than Pt polycrystalline, modifying the electronic environment and therefore changing the adsorption strength of hydrogen. Moreover, Figure 8 shows that S1 and S2 do not exhibit a peak oxidation between 0.4 and 0.45 V in contrast to S3, which is due to the possible presence of the Fe atoms on the surfaces of the Pt nanoparticles, which promotes an increase of adsorption of OH-species on the surface of the nanoparticles [36]. Moreover, in Figure 8, in the cathodic scan it can be observed a shift of 0.1 V in the peak of the OH-desorption species for S3, in relation with the others samples, which indicates that the

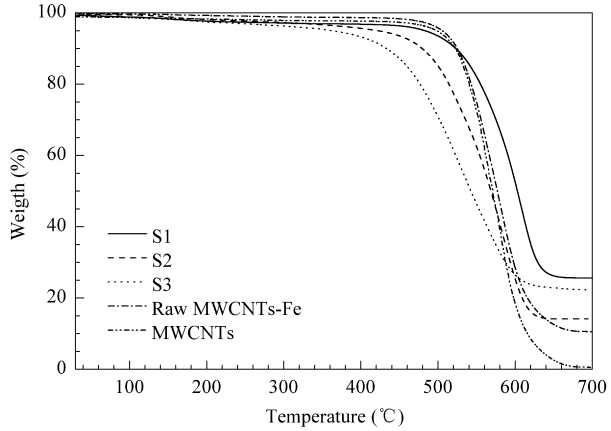

Figure 7. TGA analyses under dry air flux for the different Pt-M/MWCNTs systems

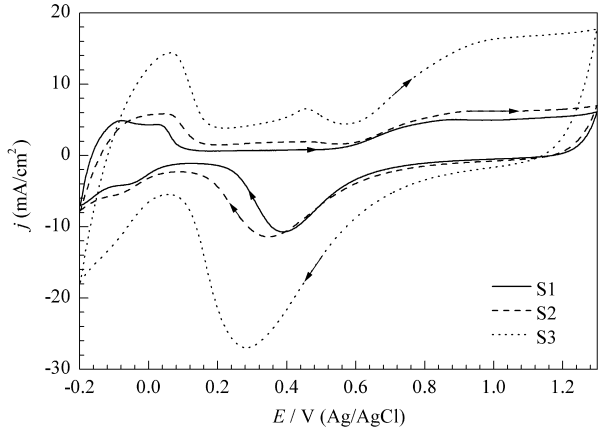

Figure 8. Cyclic voltammograms of electrocatalysts in a 0.5 mol/L H_2SO_4 solution saturated with N_2 with a scan rate of 100 mV/s

OH-species are more strongly adsorbed on the surface of the nanoparticles. This is due to the Pt-Fe material which is more electropositive.

3.4.1. Methanol oxidation

Figure 9 shows the cyclic voltammograms obtained for the methanol oxidation reaction of the electrocatalysts. The detailed analysis for the methanol oxidation reaction is summarized in Table 6. It can be observed that during the anodic scan, the current rapidly increases forming a peak in about 1.0, 1.2 and 0.6 V for S1, S2 and S3, respectively, which are attributed to the MeOH electrooxidation in forward scan. After cathodic scan, the current increases due to the carbonaceous species oxidation in the back scan [37], forming peaks around 0.56, 0.7 and 0.43 V for S1, S2 and S3, respectively. Table 6 summarizes the oxidation peaks obtained for the samples in the methanol oxidation reaction. According to these results, the bimetallic systems S1 and S3 showed a good electroactivity. The relation j_f/j_b indicates whether the material is a resistant electrocatalyst to CO poisoning in methanol oxidation. Figure 9 shows that the catalyst S3 records the highest ratio of electroactivity with a j_f/j_b of 1.5, recording a higher oxidation current density (j_f) with a value of 86 mA·cm^{-2} at 0.618 V. Furthermore, S3 starts the MOR around 0.3 V, this being the lowest value. Moreover, it can be observed that S3 oxidizes the carbonaceous species in the cathodic scan at the lowest potential of 0.437 V. It is believed that this improvement in the electroactivity of S3 is due to the presence of Fe atoms on the surface of the Pt nanoparticles. Moreover, it is believed that the presence of Fe nanoparticles in the MWCNTs promotes a shift in the oxidation potential because S1 shows a peak of MOR at 0.99 V, which is lower than that presented by S2 at 1.24 V.

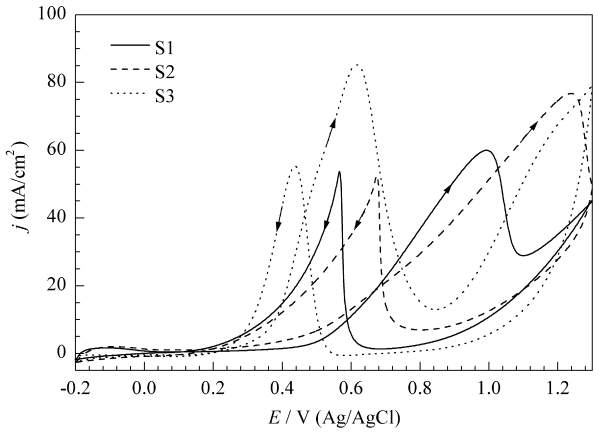

Figure 9. Cyclic voltammograms of methanol oxidation of three electrocatalysts performed in a 1.0 mol/L MeOH+0.5 mol/L H_2SO_4 solution saturated with N_2 at room temperature at a scan rate of 100 mV/s

For further assess, the electrocatalyst performance toward MeOH oxidation was carried out with chronoamperometry tests at a steady potential. Figure 10 shows the CA curves corresponding to the composites, obtained in 1 mol/L MeOH+0.5 mol/L H_2SO_4 at an anodic potential of E_f. S3 was the electrocatalyst that showed the highest current density throughout the experiment in comparison with the other samples. Moreover, from these results poisoning rates were determined [38], S1 and S2 having similar poisoning rates of 0.2993 min^{-1} and 0.2881 min^{-1}, respectively. Furthermore, S3 exhibited a very low poisoning rate of 3.7049×10^{-7} min^{-1}. These results are consistent with the cyclic voltammograms obtained wherein S3 presented a very high activity compared with the S1 and S2 systems, which is an indication that S3 is an excellent electrocatalyst for methanol electrooxidation.

Table 6. Oxidation peaks of cyclic voltammogram of the electrocatalysts systems

Samples	E_f (mV)	j_f	E_b (mV)	j_b	j_f/j_b
S1	991	60	566	55	1.1
S2	1238	76	675	53	1.4
S3	618	86	437	56	1.5

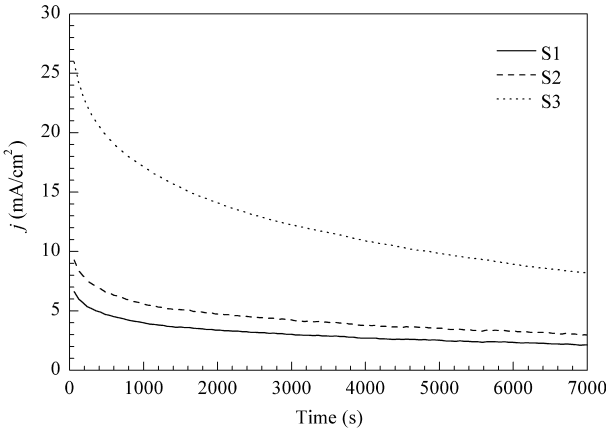

Figure 10. Chronoamperommetry of methanol oxidation at E_f vs Ag/AgCl for three electrocatalysts systems in 1 mol/L MeOH+0.5 mol/L H_2SO_4 solution saturated with N_2 at room temperature

4. Conclusions

Results obtained in this work imply that the Pt-Fe/MWCNTs system has adequate potential applications for fuel cells. The reduction of its particle size to the nanoscale leads to an increase of the catalytic sites/unit mass; however, it may be coupled with a structural change in the increase of the turnover number for certain structure-sensitive reactions. It was shown that adsorbed hydrogen exhibited a strong dependence on factors such as particle size and surface composition. The structures may play a more important role in the hydrogen adsorption and desorption than the compositions of the Pt-Fe nanoparticle catalysts.

Acknowledgements

We gratefully acknowledge for their technical support to I. Gradilla, Fco. Ruiz, E. Aparicio and J. Peralta from CNyN-UNAM. We also thank CONACyT (Project 155388 and 174689) for its financial support.

References

[1] Jung D H, Bae S J, Kim S J, Nahm K S, Kim P. *Int J Hydrogen Energy*, 2011, 36(15): 9115
[2] Esmaeilifar A, Rowshanzamir S, Eikani M H, Ghazanfari E. *Energy*, 2010, 35(9): 3941
[3] Zeng J H, Lee J Y. *Int J hydrogen Energy*, 2007, 32(7): 4389
[4] Huang H J, Chen H Q, Sun D P, Wang X. *J Pow Sources*, 2012, 204(1): 46
[5] Li W Z, Xin Q, Yan Y S. *Int J hydrogen Energy*, 2010, 35(6): 2530
[6] Lin J F, Kamavaram V, Kannan A M. *J Pow Sources*, 2010, 195(2): 466
[7] Bashyam R, Zelenay P. *Nature*, 2006, 443(7107): 63
[8] Othman R, Dicks A L, Zhu Z H. *Int J Hydrogen Energy*, 2012, 37(1): 357
[9] Lamy C, Lima A, LeRhun V, Delime F, Coutanceau C, Leger J M. *J Pow Sources*, 2002, 105(2): 283
[10] Jusys Z, Kaiser J, Behm R J. *Electrochim Acta*, 2002, 47(22-23): 3693
[11] Ye W C, Kou H H, Liu Q Z, Yan J F, Zhou F, Wang C M. *Int J Hydrogen Energy*, 2012, 37(5): 4088
[12] Guo S J, Wang E K. *Nano Today*, 2011, 6(3): 240
[13] Li L, Xing Y C. *J Phys Chem C*, 2007, 111(6): 2803
[14] Wu P, Li B H, Du H D, Gan L, Kang F Y, Zeng Y Q. *J Power Sources*, 2008, 184(2): 381
[15] Liu X, Villacorta R, Adame A, Kannan A M. *Int J Hydrogen Energy*, 2011, 36(17): 10877
[16] Kruusenberg I, Matisen L, Shah Q, Kannan A M, Tammeveski K. *Int J Hydrogen Energy*, 2012, 37(5): 4406
[17] Alonso-Nuñez G, de la Garza L M, Rogel-Hernandez E, Reynoso E, Licea-Claverie A, Felix-Navarro R M, Berhault G, Paraguay-Delgado F. *J Nanopart Res*, 2011, 13(9): 3643
[18] Rodriguez J R, Félix R M, Reynoso E A, Moyado S F, Alonso-Núñez G. *Inorg Chim Acta*, 2013, 406: 138
[19] Yang J, Lee J Y, Ying J Y. *Chem Soc Rev*, 2011, 40(3): 1672
[20] Aguilar-Elguezabal A, Antúnez W, Alonso G, Delgado F P, Espinosa F, Miki-Yoshida M. *Diamond Relat Mater*, 2006, 15(9): 1329
[21] Solla-Gullon J, Rodríguez P, Herrero E, Aldaz A, Feliu J M. *Phys Chem Chem Phys*, 2008, 10(10): 1359
[22] Habibi B, Delnavaz N. *Int J Hydrogen Energy*, 2011, 36(16): 9581
[23] Khorasani-Motlagh M, Noroozifar M, Ekrami-Kakhki M S. *Int J Hydrogen Energy*, 2011, 36(18): 11554
[24] Ye W C, Kou H H, Liu Q Z, Yan J F, Zhou F, Wang C M. *Int J Hydrogen Energy*, 2012, 37(5): 4088
[25] Nair S S, John S A, Sagara T. *Electrochim Acta*, 2009, 54(27): 6837
[26] Lehman J H, Terrones M, Mansfield E, Hurst K E, Meunier V. *Carbon*, 2011, 49(8): 2581
[27] Paul S, Samdarshi S K. *New Carbon Mat*, 2011, 26(2): 85
[28] Reddy K R, Sin B C, Yoo C H, Park W J, Ryu K S, Lee J S, Sohn D W, Lee Y I. *Scrip Mat*, 2008, 58(11): 1010
[29] Dresselhaus M S, Dresselhaus G, Jorio A, Souza A G, Saito R. *Carbon*, 2002, 40(12): 2043
[30] Belin T, Epron F. *Mat Sci Eng B*, 2005, 119(2): 105
[31] Kim K K, Park J S, Kim S J, Geng H Z, An K H, Yang C M, Sato K, Saito R, Lee Y H. *Phys Rev B*, 2007, 76(20): 205426
[32] McBrige J R, Graham G W, Peter C R, Weber W H. *J Appl Phys*, 1991, 69(3): 1596
[33] Zak A K, Abd Majid W H, Abrishami M E, Yousefi R, Parvizi R. *Solid State Sci*, 2012, 14(4): 488
[34] Pozio A, De Francesco M, Cemmi A, Cardellini F, Giorgi L. *J Power Sources*, 2002, 105(1): 13
[35] Sellin R, Clacens J M, Coutanceau C. *Carbon*, 2010, 48(8): 2244
[36] Lei T, Zei M S, Ertl G. *Surf Sci*, 2005, 581(2-3): 142
[37] Manoharan R, Goodenough J B. *J Mater Chem*, 1992, 2(8): 875
[38] Green C L, Kucernak A. *J Phys Chem B*, 2002, 106(44): 11446